Supporting Information

Quantitative Analysis of Different Formation Modes of Platinum Nanocrystals Controlled by Ligand Chemistry

X. Yin[1], M. Shi[1], J. Wu[1], Y.-T. Pan[1], D. L. Gray[2], J. A. Bertke[2], H. Yang[1]*

[1]Department of Chemical and Biomolecular Engineering, University of Illinois at Urbana-Champaign, 206 Roger Adams Laboratory, 600 S. Matthews Avenue, Urbana, IL 61801, USA

[2] George L. Clark X-Ray Facility, University of Illinois at Urbana-Champaign, 505 S. Matthews Avenue, Urbana, IL 61801, USA

* Corresponding author. Email: hy66@illinois.edu

This file includes:

Materials and Methods

Materials. Platinum (II) acetylacetonate ($Pt(acac)_2$, 98%, Strem Chemicals, Inc), oleylamine (OAm, 70%, Aldrich), oleic acid (OA, 90%, Aldrich), acetic acid (HOAc, 99.7%, J. T. Baker), propionic acid (PA, 99.5%, Aldrich), butylamine (BAm, 99.5%, Aldrich), acetylacetone (acacH, 99.6%, analytical standard, Fluka), carbon monoxide (CO, 99.998%, S.J. Smith Co.), argon (Ar, S.J. Smith Co.), chloroform (99.8%, Fisher Scientific), and ethanol (200 proof, Decon Labs, Inc) were used as received.

Synthesis of Pt nanocrystals with ligand-tuned Pt precursor. In a typical synthesis, 20 mg of $Pt(acac)_2$ (0.051 mmol) was used as the precursor. Various amounts of OA was added into 9 mL of degassed OAm (27.4 mmol) and used as the solvent to achieve various molar ratios of OA:$Pt(acac)_2$. For instance, OA-to-$Pt(acac)_2$ molar ratio of 4:1 can be achieved with the addition of 70 μL of OA (0.22 mmol). After the addition of 20 mg $Pt(acac)_2$ (0.051 mmol), the mixture was preheated at 80 °C for 20 min under magnetic stirring at 300 rpm to allow the complexation of $Pt(acac)_2$ with OAm/OA till a quasi-equilibrium state was achieved. The mixture was then immersed in oil bath at 210 °C with 300 rpm magnetic stirring and carbon monoxide (CO) was bubbled through the mixture at 110 cm^3/min to reduce the Pt precursor. During the reaction, aliquots were taken at sequential time intervals and quenched to room temperature in glass vials immersed in cold water. The aliquots were then washed with chloroform and ethanol (volume ratio 1:5) and centrifuged at 12000 rpm for 10 min to collect Pt nanocystals. The supernatants were transparent and varied in colors. Pt nanoparticles were precipitated on the centrifuge tube walls and then re-dispersed into chloroform for further characterization.

UV–vis absorption spectroscopy analysis. A Carry 60 UV–vis spectrometer (Agilent) was used for this analysis. Chloroform was used as solvent and pure chloroform was scanned as the background. During the synthesis, samples with 20 μL volume were taken from the quenched aliquots and diluted with 4 mL chloroform. For the aliquots of Pt/OAm/OA complex samples, 10 μL of aliquots were first diluted with 1 mL chloroform, and then 20 μL of diluted solution was further diluted into 4 mL of chloroform for UV–vis spectroscopy analysis.

To study the reaction between acacH with OAm and OA, 5.1 μL of acacH (0.05 mmol) was added into 33 μL of OAm (0.1 mmol), or into the mixture of OAm (66 μL or 0.2 mmol) and OA (32 μL or 0.1 mmol), capped and heated at 80 °C for 20 min. The obtained solutions were then diluted with 9 mL chloroform. For UV–vis spectroscopy analysis, 40 μL of samples were further diluted with 4 mL of chloroform. The final equivalent concentration of acacH in chloroform was 5.5×10^{-2} mM. Chloroform solution of acacH at same equivalent concentration was also characterized for comparison. In addition, 20 μL of OAm, or 20 μL of the mixture of OAm (10 mL) and OA (100 μL) was also diluted with 4 mL of chloroform for UV–vis spectroscopy analysis. The equivalent concentration of OAm was around 15.2 mM.

Mass spectrometry study of controlled Pt complex formation. To study complexation of $Pt(acac)_2$ with OAm and OA, $Pt(acac)_2$ (39.4 mg or 0.1 mmol) was added to OAm (329 μL or 1 mmol), or a mixture of OAm (428 μL or 1.3 mmol) and OA (96 μL or 0.3 mmol) heated at 130 °C for 5 min. 1 μL obtained mixture was dissolved in 90 μL chloroform and submitted for mass spectrometry analysis. The samples were characterized

using an UltrafleXtreme matrix assisted laser deposition/ionization time-of-flight (MALDI–TOF) mass spectrometer (Bruker Daltonics). ChemDraw (Cambridge Software) was used to calculate the isotopic mass distribution of proposed complexes for further comparison with the experimental data.

Synthesis and crystallization of $[Pt(NH_2C_4H_7)_4](OOCCH_3)_2$ ($[Pt(BAm)_4]^{2+}(OAc^-)_2$, compound 1). In this study, 394 mg of $Pt(acac)_2$ was mixed with 2.5mL of BAm and 516 μL of HOAc in a closed glass vial in Ar and heated and stirred at 130 °C for 5 min. After cooling the solution down to room temperature, hexane was added into the solvent to extract and purify the product. The obtained yellow solution was then vacuumed to remove excess solvent and byproducts. The condensed solution was dissolved in toluene and crystallized at room temperature by slow evaporation of solvents. The obtained single crystals were submitted for single crystal x-ray diffraction.

Synthesis and crystallization of $[Pt(NH_2C_4H_7)_4](OOCCH_2CH_3)_2$ ($[Pt(BAm)_4]^{2+}(PA^-)_2$, compound 2). In this study, 788 mg of $Pt(acac)_2$ was mixed with 3.9 mL of BAm and 670 μL of PA in a closed glass vial in Ar and heated and stirred at 130 °C for 5 min. After cooling down to room temperature, hexane was added into the solvent to extract and purify the product. The obtained yellow solution was then vacuumed to remove excess solvent and byproducts. The condensed solution was then dissolved in hexane and crystallized at room temperature by slow evaporation of solvents.

Synthesis and crystallization of $[Pt(NH_2C_4H_7)_4](C_5H_7O_2)_2$ ($[Pt(BAm)_4]^{2+}(acac^-)_2$, compound 3). In this study, 394 mg of $Pt(acac)_2$ was mixed with 2.5 mL of BAm in a closed glass vial in Ar and heated and stirred at 130 °C for 5 min. After cooling down to room temperature, hexane was added into the solvent to extract and purify the product. The obtained yellow solution was then vacuumed to remove excess solvent and byproducts. The crystals are crystallized in toluene, with the similar method as described above.

X-ray Crystallography. Single crystal X-ray diffraction data were collected with the use of graphite-monochromatized Cu Kα radiation (1.54178 Å) on a Bruker APEX II CCD diffractometer[1] for compounds **1** and **2**. Data for compound **3** were collected with Mo Kα radiation (0.71073 Å) on a Bruker SMART/APEX II CCD diffractometer[1]. Combinations φ and ω scans were used to collect the data. The collection, cell refinement and integration of intensity data was carried out with the APEX2 software[1]. Face-indexed absorption corrections were performed numerically with XPREP[2]. Then SADABS[3] was employed to make incident beam corrections. The structure was solved with the direct methods SHELXS[4] and refined with the full-matrix least-squares SHELXL[5] program. Additional metrical details are available in Table SI. CCDC 1484407, 1484408, and 1484409 contain the supplementary crystallographic data for **2**, **3**, and **1** respectively. These data can be obtained free of charge from the Cambridge Crystallographic Data Centre via www.ccdc.cam.ac.uk/structures.

Transmission electron microscopy (TEM) characterization of Pt Nanocrystals. To study the growth kinetics of Pt nanocrystals, aliquots were taken during the reaction at different time point. The samples were first washed with chloroform and ethanol, then dispersed in chloroform and further dried on copper grids for TEM characterization. A

JEOL 2100 Cryo TEM with an accelerating voltage of 200 kV and equipped with Gatan 2K×2K CCD was used. The samples were browsed in TEM at low magnifications to examine the uniformity of the Pt NCs. Micrographs of representative areas covered with nanoparticles were taken for further analysis. Size distribution of Pt nanoparticles was evaluated by measuring the projected areas (A, nm^2) of more than 200 nanoparticles with the software ImageJ from TEM micrographs. According to the shapes of the particles, the projected areas of individual particles were converted into particle volumes (V, nm^3) using the necessary formula. For spherical shape, $V = 4/3\, A^{1.5}\, \pi^{-0.5}$ was used, and for cubic shape, $V = A^{1.5}$ was used.

Correlating averaged particle size with kinetic data. Aliquots were centrifuged and the supernatants were submitted for inductively coupled plasma optical emission spectroscopy (ICP–OES) measurement using an Optima 2000DV (PerkinElmer) to determine the yield of Pt nanocrystals. ICP-OES data were then correlated with the average volumetric particle size at the same reaction times, and the whole particle-size-time plot was converted into a kinetic plot for the reaction. The obtained data was further fitted to different reaction models to calculate the kinetic constants. ICP–OES measurements showed that the yields of Pt were 95.4% at 5 min with OA:$Pt(acac)_2$ molar ratio of 0:1, 31.8% at 30 min with OA:$Pt(acac)_2$ molar ratio of 1.7:1, and 11.8% at 50 min with OA:$Pt(acac)_2$ molar ratio of 4:1.

We assumed that the number density of nanoparticles in solution was constant during the reaction. This assumption is based on two reasons: 1) the samples are statistically uniform in size and no new nuclei were observed in the product within the growth stage studied here; 2) previous *in situ* TEM studies also suggest that the change of nuclei number density due to coalescence happens at the very early stages of the reaction (< 100 s), after which the number density of nanoparticles remain constant in the later growth stages[6]. Therefore the particle number density (n) is constant in each group and the following relations hold true:

$$n = \frac{N}{V} \tag{S1}$$

$$y = \frac{N \times \bar{V}_{NP} \times \rho}{w_{\mathrm{Pt}}^{0}} \times 100\% \tag{S2}$$

$$y \propto \bar{V}_{NP} \tag{S3}$$

where N is the total number of nanoparticles in the solution with volume V, n is the number density of nanoparticles, y is the yield of Pt nanoparticles, $\bar{V}_{NP}$ is the average particle size measured in volume, ρ is the density of bulk Pt, w_{Pt}^{0} is the initial total weight of Pt metal in the system, which is 9.9 mg. The shapes of nanoparticles were approximated to spheres and cubes accordingly based on their morphologies observed using TEM. The volumetric size of each particle was then calculated based on their projected area and the geometry formulas of sphere and cube.

Growth Kinetic Models.
We developed three kinetic models to describe the growth mechanisms of the system.

I: Two-step mechanism:

We developed a modified pseudo two-step mechanism based on the Finke-Watzky model[7]:

$$A \xrightarrow{k_1} B \tag{S4}$$

$$A + B_{surface} \xrightarrow{k_2} 2B \tag{S5}$$

where A is the Pt precursor, B is the active site on Pt nanocrystals measured by the surface area of Pt nanocrystal in per unit volume of solution. k_1 and k_2 are the rate constants of these steps. To capture the surface-autocatalytic character of the reaction, we used the surface area of B per volume of solution, denoted as $[B_{surface}]$:

The differential equation can be expressed as follows:

$$-\frac{d[A]}{dt} = \frac{d[B]}{dt} = k_1[A] + k_2[A][B_{surface}] \tag{S6}$$

$$[B_{surface}] = (\frac{[B]}{n\rho})^{2/3} Fn = (\frac{[B]}{\rho})^{2/3} Fn^{1/3} \tag{S7}$$

where $[B_{surface}]$ is the surface area of Pt nanocrystals in a unit volume, F is the surface area to volume ratio for a unit volume, n is the number density of nanoparticles, ρ is the density of bulk Pt. F is equal to 6 for cubic shape and 4.836 for quasi-spherical shape.

$$\frac{d[B]}{dt} = k_1[A] + k_2[A](\frac{[B]}{\rho})^{2/3} Fn^{1/3} \tag{S8}$$

$$\frac{dy}{dt} = k_1(1-y) + \frac{k_2 Fn^{1/3}}{\rho^{2/3}}[A]_0^{2/3}(1-y)y^{2/3} \tag{S9}$$

If a new parameter, k'_2, is set to be:

$$k'_2 = \frac{k_2 Fn^{1/3}}{\rho^{2/3}}[A]_0^{2/3} \tag{S10}$$

then the Equation (S9) can be written as the following:

$$\frac{dy}{dt} = k_1(1-y) + k'_2(1-y)y^{2/3} \tag{S11}$$

II: One-step mechanism:

When the autocatalytic reaction pathway is inhibited, the system can be described by a one-step mechanism. In this model, the precursor A is decomposed through a first-order step into B (Pt(0)) and deposited rapidly onto the existing Pt nanocrystals. The decomposition step is the rate limiting step.

$$\mathrm{A} \xrightarrow{k_1} \mathrm{B} \tag{S12}$$

$$-\frac{d[\mathrm{A}]}{dt} = \frac{d[\mathrm{B}]}{dt} = k_1[\mathrm{A}] \tag{S13}$$

$$\frac{dy}{dt} = k_1(1-y) \tag{S14}$$

$$y = 100\% - \exp(-k_1 t) \tag{S15}$$

III: Mixed-Two-Step Mechanism:

We can modify the mixed-two-step mechanism I by introducing the surface area term [$B_{surface}$], and similar treatment as that in Eq.14:

First order reaction $\mathrm{A}_1 \xrightarrow{k_1} \mathrm{B}$ (S16)

First order reaction $\mathrm{A}_2 \xrightarrow{k_2} \mathrm{B}$ (S17)

Autocatalytic reaction $\mathrm{A}_1 + \mathrm{B}_{surface} \xrightarrow{k_3} 2\mathrm{B}$ (S18)

where A_1 and A_2 represent the two forms of Pt precursor species, $Pt(OAm)_4(acac)_2$ and $Pt(OAm)_4(OA)_2$, respectively. The completion of Pt reduction *y* can be calculated by solving the following differential equations with initial value numerically:

$$-\frac{d[\mathrm{A}]}{dt} = \frac{d[\mathrm{B}]}{dt} = k_1[\mathrm{A}_1] + k_2[\mathrm{A}_2] + k_3[\mathrm{A}_1]\left(\frac{[\mathrm{B}]}{\rho}\right)^{2/3} Fn^{1/3} \tag{S19}$$

$$-\frac{d[\mathrm{A}_2]_t}{dt} = k_2[\mathrm{A}_2] \tag{S20}$$

$$[\mathrm{A}] = [\mathrm{A}_1] + [\mathrm{A}_2] = [\mathrm{A}]_0 - [\mathrm{B}] \tag{S21}$$

$$C = \frac{[\mathrm{A}_2]_0}{[\mathrm{A}]_0} \tag{S22}$$

$$\frac{dy}{dt} = k_1[100\% - y - C\exp(-k_2 t)] + k_2 C\exp(-k_2 t) + k'_3\, y^{2/3}[100\% - y - C\exp(-k_2 t)]$$

(S23)

$$k'_3 = \frac{k_3 F n^{1/3}}{\rho^{2/3}}[\mathrm{A}]_0^{2/3} \qquad \text{(S24)}$$

Supplementary Figures

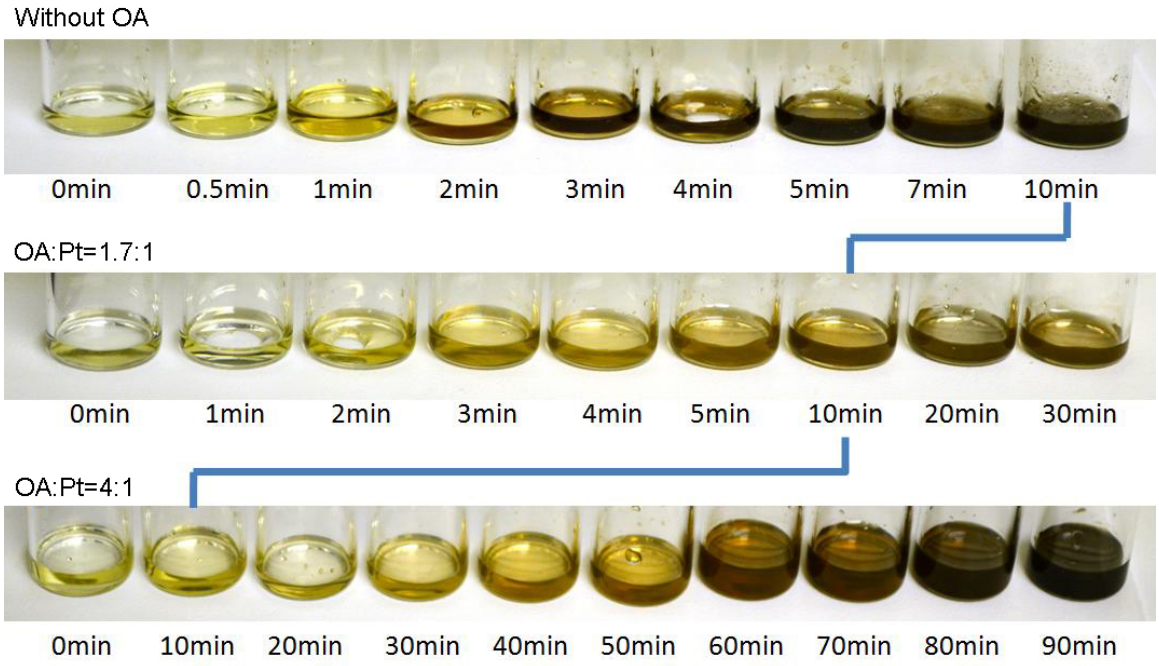

Fig. S1. Color change of the reactant mixture of $Pt(acac)_2$, OAm and OA with the reaction time.

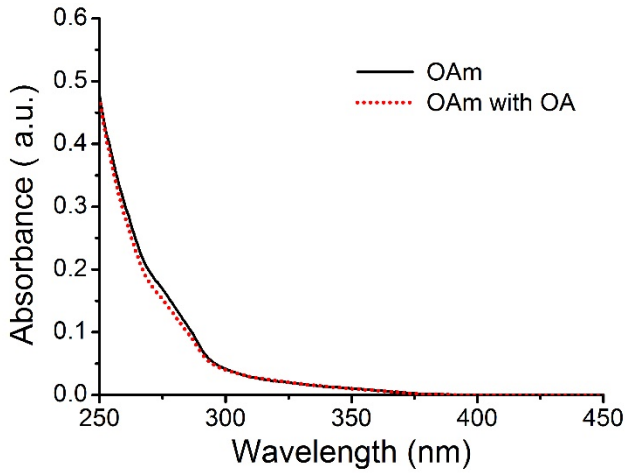

Fig. S2. UV–vis spectra of OAm and a mixture of OAm and OA in chloroform.

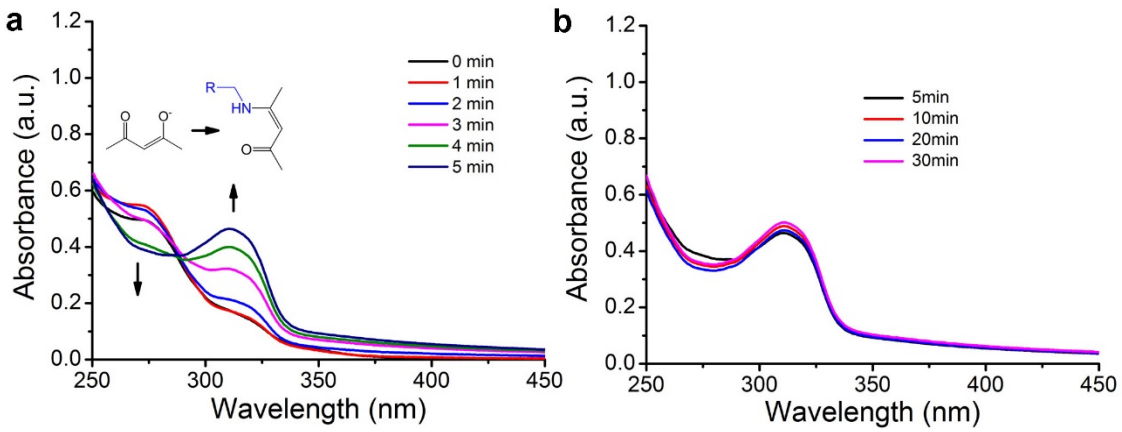

Fig. S3. UV–vis spectra of $Pt(acac)_2$ in OAm without OA during the reaction for a time period of **a**, 0 to 5 min; and **b**, 5 to 30 min, respectively.

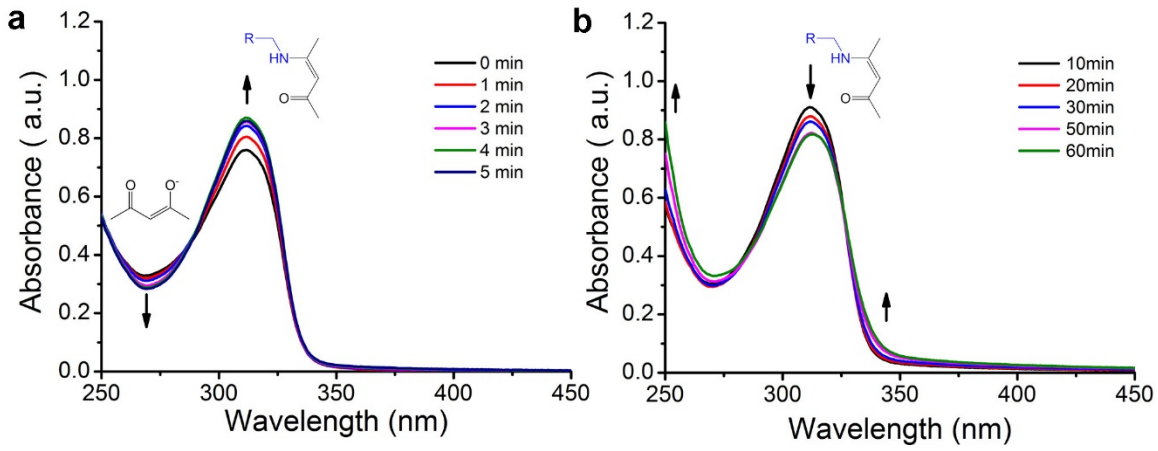

Fig. S4. UV–vis spectra of mixtures of $Pt(acac)_2$ in OAm at OA:$Pt(acac)_2$ molar ratio of 1.7:1 for the reaction of a time period of **a**, 0 to 5 min; and **b**, 10 to 60 min, respectively.

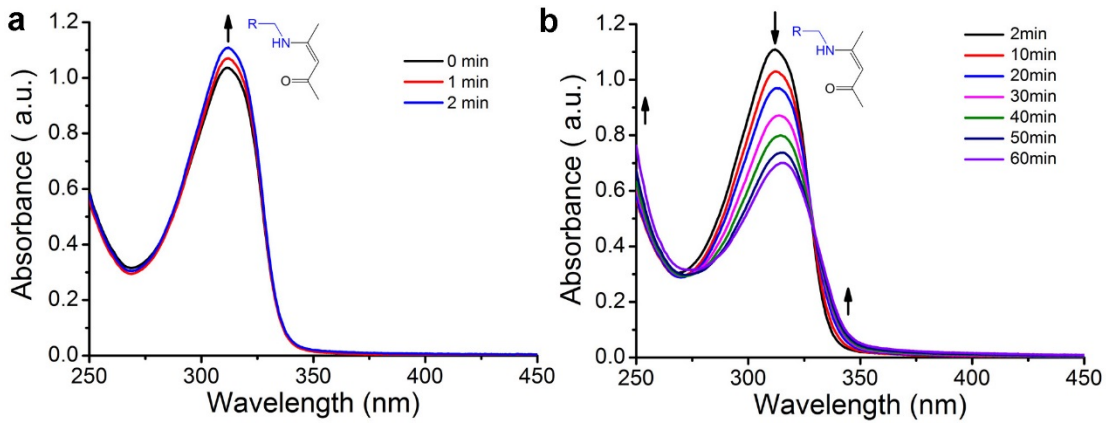

Fig. S5. UV–vis spectra of of mixtures of $Pt(acac)_2$ in OAm at OA:$Pt(acac)_2$ molar ratio of 4:1 for the reaction of a time period of **a**, 0 to 2 min; and **b**, 2 to 60 min, respectively.

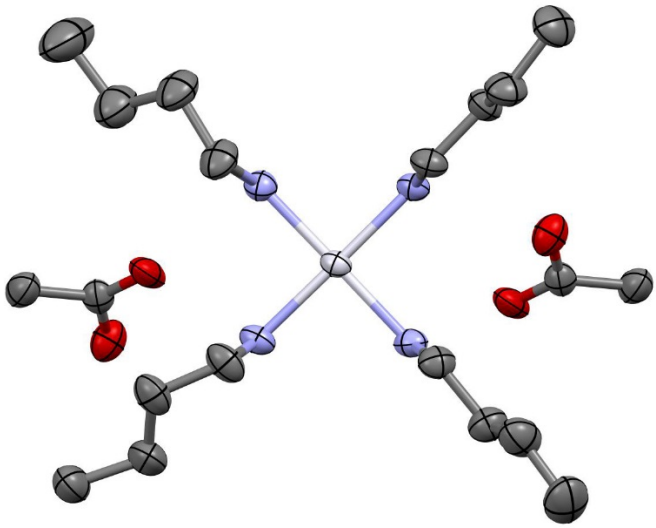

Fig. S6. Thermal ellipsoid plot of ([Pt (BAm)$_4$]$^{2+}$ (OAc$^-$), **1**) as identified from X-ray diffraction analysis. Platinum: silver; carbon: gray; oxygen: red; nitrogen: blue. (Ellipsoids set at 50% probability; H atoms are omitted for clarity).

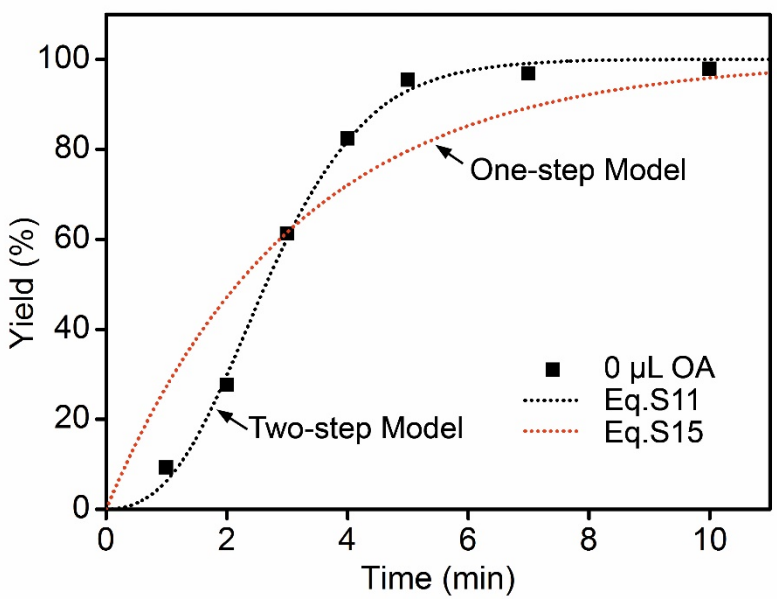

Fig. S7. Kinetic analysis of the reaction in the presence of OAm (no OA) using different models to fit the curves. The two-step mechanism (Eq.S11) fits well to the data, while the one-step mechanism (Eq. S15) fails.

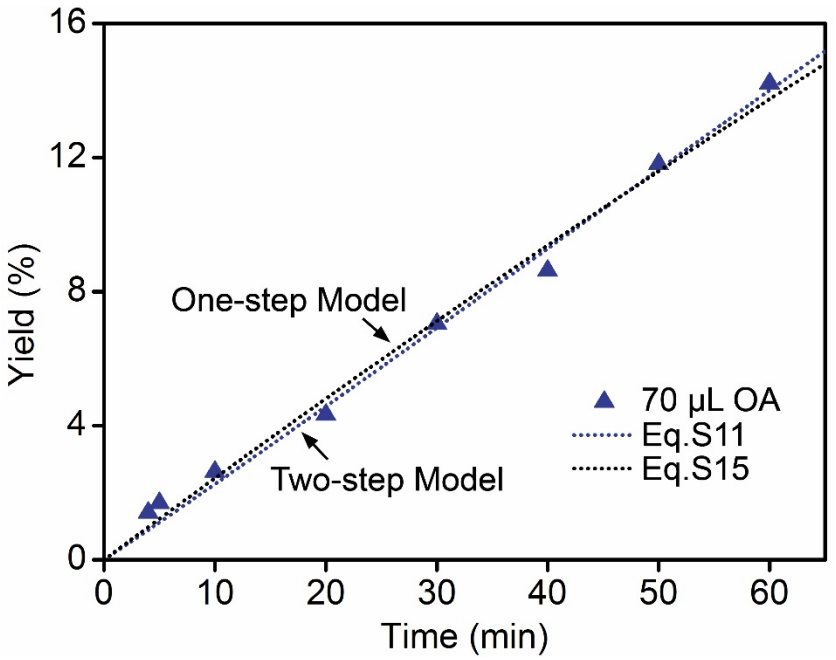

Fig. S8. Kinetic analysis of the reaction in the system with OA:$Pt(acac)_2$ molar ratio of 4:1 using the two different models. Both the two-step (Eq. S11) and one-step mechanisms (Eq.S15) fit the data well.

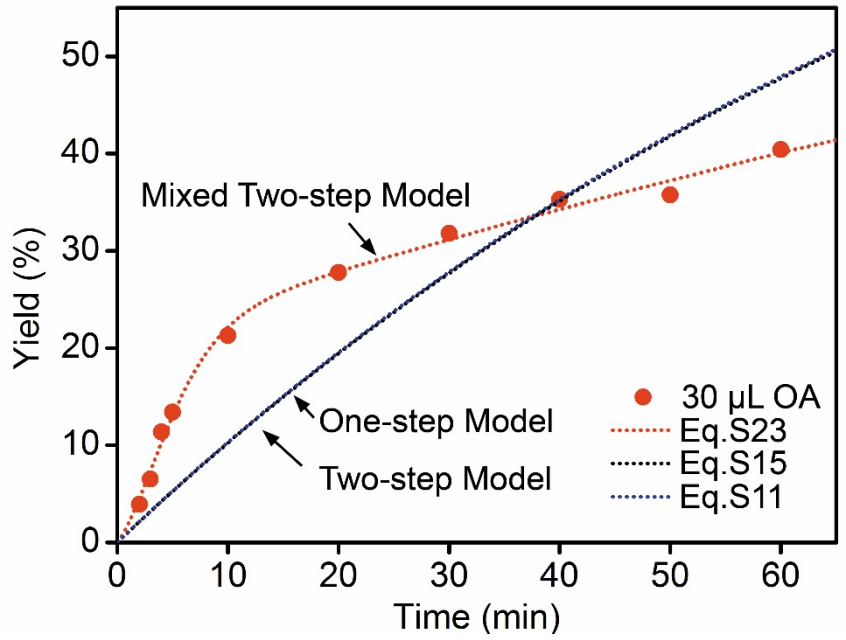

Fig. S9. Kinetic analysis of the reaction in the system with OA:$Pt(acac)_2$ molar ratio of 1.7:1 using various different models. The mixed-two-step mechanism (Eq. S23) fits well to the data. The two-step mechanism (Eq. S11) and one-step mechanism (Eq. S15) fail.

Table S1. Crystal data and structure refinement details for compounds **1**, **2** and **3**

Molecule	$([Pt(BAm)_4]^{2+}(OAc^-)_2$, **1**)	$([Pt(BAm)_4]^{2+}(PA^-)_2$, **2**)	$([Pt(BAm)_4]^{2+}(acac^-)_2$, **3**)
Empirical formula	C20 H52 N4 O5 Pt	C22 H54 N4 O4 Pt	C26 H58 N4 O4 Pt
Formula weight	623.74	633.78	685.85
Temperature	183(2)k	273(2) K	186(2) K
Wavelength	1.54178 Å	1.54178 Å	0.71073 Å
Crystal system	Triclinic	Triclinic	Monoclinic
Space group	P-1	P-1	C2/c
Unit cell dimensions			
a	13.7655(7) Å	13.5414(11) Å	24.952(4) Å
b	13.8230(7) Å	14.4168(12) Å	15.408(2) Å
c	18.2522(9) Å	16.4731(14) Å	19.431(3) Å
α	105.802(2)°	100.681(4)°	90°
β	95.300(2)°	90.941(4)°	115.918(2)°
γ	116.4880(10)°	96.678(4)°	90°
Volume	2897.3(3) $Å^3$	3136.4(5) $Å^3$	6719.2(17) $Å^3$
Z	4	4	8
Density (calculated)	1.430 Mg/m^3	1.342 Mg/m^3	1.356 Mg/m^3
Absorption coefficient	9.311 mm^{-1}	8.586 mm^{-1}	4.208 mm^{-1}
F(000)	1272	1296	2816
Crystal size	0.452 x 0.373 x 0.316 mm^3	0.466 x 0.233 x 0.162 mm^3	0.248 x 0.223 x 0.046 mm^3
Theta range for data collection	2.597 to 67.664°.	2.73 to 67.73°.	1.60 to 25.32°.
Index ranges	-15<=h<=16	-12<=h<=16	-29<=h<=30
	-16<=k<=15	-17<=k<=16	-18<=k<=18
	-20<=l<=21	-18<=l<=19	-23<=l<=23
Reflections collected	35583	37098	36477
Independent reflections	10041[R(int) = 0.0426]	10830 [R(int) = 0.0476]	6141 [R(int) = 0.0445]
Completeness to theta = 25.32°	95.70%	95.30%	99.90%
Absorption correction	Integration	Integration	Integration
Max. and min. transmission	0.9985 amd 0.7315	0.9985 and 0.6940	0.9985 and 0.8428
Refinement method	Full-matrix least-squares on F^2	Full-matrix least-squares on F^2	Full-matrix least-squares on F^2
Data / restraints / parameters	10041 / 1206 / 835	10830 / 1932 / 1039	6141 / 511 / 510
Goodness-of-fit on F^2	1.13	1.149	1.008
Final R indices [I>2sigma(I)]	R1 = 0.0329, wR2 = 0.0810	R1 = 0.0485, wR2 = 0.1344	R1 = 0.0202, wR2 = 0.0418
R indices (all data)	R1 = 0.0339, wR2 = 0.0819	R1 = 0.0851, wR2 = 0.1824	R1 = 0.0330, wR2 = 0.0462
Largest diff. peak and hole	0.884 and -2.218 $e.Å^{-3}$	0.838 and -1.576 $e.Å^{-3}$	0.487 and -0.434 $e.Å^{-3}$

References

1. Bruker, A. *APEX 2*. Bruker Axs Inc.: Madison, Wisconsin, USA, **2004**.

2. Bruker, A. *SAINT, SHELXTL, XCIF, XPREP*. Bruker Axs Inc.: Madison, Wisconsin, USA, **2005**.

3. Sheldrick, G. M. *SADABS*. Bruker Axs Inc.: Madison, Wisconsin, USA, **2007**.

4. Sheldrick, G. M. *SHELXS-97, Program for the solution of Crystal Structure*. University of Göttingen, Germany, **1997**.

5. Sheldrick, G. M. *SHELXL-97, Program for structure refinement*. University of Göttingen, Germany, **1997**.

6. Zheng, H.; Smith, R. K.; Jun, Y.-w.; Kisielowski, C.; Dahmen, U.; Alivisatos, A. P. *Science* **2009,** *324*, 1309–1312.

7. Watzky, M. A.; Finke, R. G. *J. Am. Chem. Soc.* **1997,** *119*, 10382–10400.